Bond Length Alternation and Internal Dynamics in Model Aromatic Substituents of Lignin

A. O. Hernandez-Castillo,[a,b] Camilla Calabrese,[c,d,e] Sean M. Fritz,[a] Iciar Uriarte,[c] Emilio J. Cocinero*[c,d] and Timothy S. Zwier*[a,f]

[a] Dr. A. O. Hernandez-Castillo, Dr. S. Fritz, Prof. T. Zwier
Department of Chemistry
Purdue University
West Lafayette, IN 47907-2084, USA
[b] Dr. A. O. Hernandez-Castillo
Department of Molecular Physics
Fritz Haber Institute of the Max Planck Society
Faradayweg 4-6, Berlin, Germany, D-14195
[c] Dr. C. Calabrese, Dr. I. Uriarte, Dr. E.J. Cocinero
Department of Physical Chemistry, Faculty of Science and Technology
University of the Basque Country (UPV/EHU)
Bº Sarriena, S/N, Leioa 48940, Spain
[d] Dr. C. Calabrese, Dr. E.J. Cocinero
Instituto Biofisika (UPV/EHU-CSIC)
University of the Basque Country (UPV/EHU)
Bº Sarriena S/N, Leioa 48940, Spain
E-mail: emiliojose.cocinero@ehu.es
[e] Dr. C. Calabrese
Fundación Biofísica Bizkaia/Biofisika Bizkaia Fundazioa (FBB),
E-48940, Leioa (Spain)
[f] Prof. T. Zwier
Gas Phase Chemical Physics,
Livermore, CA 94550, USA
E-mail: tszwier@sandia.gov

Supporting information for this article is given via a link at the end of the document.

Abstract: Broadband microwave spectra were recorded over the 2-18 GHz frequency range for a series of four model aromatic components of lignin; namely, guaiacol (*ortho*-methoxy phenol, **G**), syringol (2,6-dimethoxy phenol, **S**), 4-methyl guaiacol (**MG**), and 4-vinyl guaiacol (**VG**), under jet-cooled conditions in the gas phase. Using a combination of ^{13}C isotopic data and electronic structure calculations, distortions of the phenyl ring by the substituents on the ring are identified. In all four molecules, the $r_{C(1)-C(6)}$ bond between the two substituted C-atoms lengthens, leading to clear bond alternation that reflects an increase in the phenyl ring resonance structure with double bonds at $r_{C(1)-C(2)}$, $r_{C(3)-C(4)}$ and $r_{C(5)-C(6)}$. Syringol, with its symmetric methoxy substituents, possesses a microwave spectrum with tunneling doublets in the *a*-type transitions associated with H-atom tunneling. These splittings were fit to determine a barrier to hindered rotation of the OH group of 1975 cm^{-1}, a value nearly 50% greater than that in phenol, due to the presence of the intramolecular $OH^{\cdots}OCH_3$ H-bonds at the two equivalent planar geometries. In 4-methyl guaiacol, methyl rotor splittings are observed and used to confirm and refine an earlier measurement of the three-fold barrier V_3 = 67 cm^{-1}. Finally, 4-vinyl guaiacol shows transitions due to two conformers differing in the relative orientations of the vinyl and OH groups.

Introduction

The production of biofuels from lignocellulosic residues or energy crops constitutes one of the major solutions for providing an alternative to fossil fuels.[1] Since lignin is a major byproduct of second-generation bioethanol production, it is considered as a potential source of aromatic feedstocks that could also be used as biofuels.[2] Moreover, lignin is one of the three main components of biomass and one of the most abundant naturally occurring biopolymers on Earth, accounting for 15-25% (w/w) of herbaceous biomass,[3] second only to cellulose and hemicellulose.[4] Therefore, it is important to understand the properties of lignin in order to increase the efficacy with which it can be broken down during biofuel extraction.

Lignin is an irregular biopolymer built from three closely-related phenolic monomers: the monolignols *p*-coumaryl, coniferyl, and sinapyl alcohol.[5] These three monomers are composed of aromatic rings with varying numbers of hydroxyl and methoxy substituents. Unique chemical linkages that determine many of the macroscopic properties of the lignin hold these monomers together. Since lignin is formed by a free radical process, the detailed macromolecular structure of lignin, and how it varies from plant to plant, is still an active area of investigation.[6] As the composition of lignin is very heterogeneous, it is difficult to isolate and identify a specific single unit as well as the individual unit properties.[7] For this reason, high-resolution spectroscopic techniques in the gas phase are a powerful tool in finding a strategy to recognize the proper fingerprint for each constituent of this biopolymer.

Since lignin is an aromatic-rich polymer, several studies of model lignin compounds have been performed previously based on laser techniques, including work from the Purdue group, on several phenol and alkyl phenol derivatives, guaiacol (**G**), syringol (**S**) and its *para*-methylated derivatives. This work provides information on gas-phase structures in the electronic ground and excited states of these molecules.[8] The UV spectra of **G** and **S**, which differ by a single methoxy group on the aromatic ring, were previously found to be surprisingly different, providing a basis for their potential spectroscopic recognition in lignin oligomers.[8] Cavity-based Fourier transform microwave spectroscopy measurements of **G** and several related isotopologues have recently been performed, in which the atomic coordinates of the carbon atoms have been determined.[9] Moreover, the rotationally resolved electronic spectrum of **G** of the $S_1 \leftarrow S_0$ transition had been previously registered.[10]

Rotational spectroscopy (combined with computational methods) is a powerful tool to distinguish between structurally similar molecules. The present work reports the broadband chirped-pulse Fourier transform microwave (CP-FTMW) spectra of **G**, **S**, 4-methyl guaiacol (**MG**), and 4-vinyl guaiacol (**VG**, see Scheme 1a), including multi-resonant strong-field experiments recorded under jet-cooled conditions over the 2-18 GHz frequency range.[11]

While **G** and **S** are key aromatic substituents of lignin, the *para*-substituted guaiacol derivatives have alkyl and vinyl functionality like those of the key chemical linkages between aromatic substituents in lignin. In this study, we observe how even these apparently simple monomers have features that complicate their rotational spectra, but also serve as fingerprints that are able to identify and characterize them in detail. Finally, some conclusions based on the structural effects of the substituents on the aromatic ring, and how these may affect the internal dynamics of each molecule were carried out, where some closely related molecules were included in the discussion (see Scheme 1).

Scheme 1. *(a)* Compounds studied in this work. *(b)* Some related molecules used in the discussion. The atom numbering used in this work is shown in the guaiacol (**G**) structure.

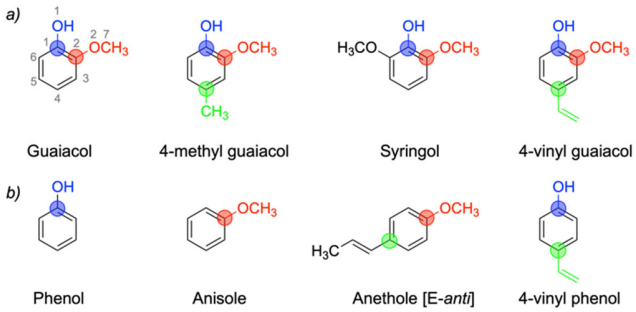

Results and Discussion

Microwave Spectra

The 2-18 GHz broadband MW spectra were obtained for all four monomers, following the details described in the Experimental Section. Moreover, the multi-resonant protocol of Strong-Field Coherence Breaking (SFCB)[11,12] was performed when necessary, in order to identify transitions due to more than one conformational isomer, thereby facilitating their assignment.
The target molecules (Scheme 1a) are calculated to be planar, and therefore possessed no μ_c component of the dipole moment. Except for **VG,** for which the alkyl chain produces *E*/*Z* conformations, the rest of the monomers (**G**, **S**, **MG**) present a simple conformational landscape characterized by a single unique structural minimum (apart from tunneling). For this reason, the conformational assignment is unambiguous, even if the presence of fine splittings due to different internal dynamic motions complicates some rotational spectra (see Internal Dynamics section).
Below, a brief description of the MW spectra of each of the four compounds is reported, including details on the type of transitions observed and the fitting results. Unless otherwise specified, rotational transition frequencies were fitted using the CALPGM program suite,[13] employing the Watson *S*-reduction and I^r representation.[14] The values of the experimental rotational constants are reported in Table 1, while the complete set of spectroscopic parameters can be found in the SI.

Guaiacol (G). Guaiacol represents a starting scaffold for the molecules studied here. As with all lignin components, the presence of the hydroxy (-OH) and methoxy (-OCH_3) groups *ortho* to one another produces a preference for an OH···OCH_3 intramolecular H-bond that lies in the plane of the phenyl ring and generally locks the molecule into a planar heavy-atom geometry.
The results obtained in this work, including ^{13}C-isotopologue data, are in keeping with the recent studys of Gurusinghe *et al*.[9] and Álvarez-Valtierra.[10] In our work, we fit a total of 158 transitions of the all ^{12}C-parent, and 22-29 transitions belonging to the seven singly ^{13}C-isotopologues ($^{13}C^{12}C_6H_8O_2$) present in natural abundance (~1.1%). In the structural discussion, we use this data to deduce the distortions in the C-atom positions in the ring.

Table 1. Experimental and theoretical rotational constants of the observed lignin analogues, calculated at the B3LYP-D3BJ/def2tzvp level. The complete set of calculated and experimental parameters can be found in SI (Tables S1-S3).

	G		**S**			
	Exp.	*Theo.*	*Exp.*	*Theo.*		
A [MHz][a]	2607.06592(51)[e]	2622	2267.07311(40)	2282		
B [MHz]	1560.79594(41)	1562	768.35079(13)	768		
C [MHz]	982.87202(39)	985	578.48124(10)	579		
σ_{fit}[b] [kHz]	12.8		11.9			
N_{Lines}[c]	158		327			
	MG		**VG**			
			***Z*-VG**		***E*-VG**	
A [MHz]	1892.95(2)	1898	1646.75211(75)	1652	1867.7943(12)	1874
B [MHz]	1168.352(3)	1172	872.49030(47)	874	779.97187(44)	782
C [MHz]	729.28(1)	731	572.90499(30)	574	552.77983(47)	554
σ_{fit} [kHz]	3.7		14		12	
N_{Lines}	173		81		45	
$N_{Population}$[d]			0.75(3)		0.25(4)	

[a] Rotational constants.
[b] Root-mean-square deviation of the fit.
[c] Number of transitions in the fit.
[d] Fractional conformational population.
[e] Error in parentheses in units of the last digit.

Syringol (S). Otherwise known as 2,6-dimethoxyphenol, **S** possesses a symmetric molecular frame due to the two methoxy groups. Its microwave spectrum was recorded with the sample holder heated between 400-420 K and entrained in 275 kPa of He. The rotational temperature of **S** following supersonic expansion was determined to be 1.7(3) K. In **S**, the internal rotation of the OH group connects two equivalent minima, giving rise to an observable tunneling splitting. Due to molecular symmetry arguments, μ_a connects rotational levels in the 0^+ and 0^- tunneling states, producing μ_a-type transitions that have an observable tunneling splitting (Figure 1b). On the other hand, μ_b connects torsional states of the same torsional symmetry and these rotational transitions are split too narrow to be resolved. The rotational constants for the two torsional substates were constrained to the same values (see details in the Internal Dynamics section), which are reported in Table 1.

***4-Methyl Guaiacol (MG)*. MG** has a methyl group on the phenyl ring, *para* to the OH substituent. The spectrum was recorded by heating the sample holder to 396 K with the sample entrained in 70 kPa of He. The rotational temperature was determined to be 1.8(3) K. As expected, a single conformer was observed stabilized by an $OH\cdots OCH_3$ intramolecular H-bond. The presence of the methyl group causes an observable splitting due to the methyl internal rotation V_3 (see Figure S1), which has been fit to determine its barrier height (see Internal Dynamics section).

4-Vinyl Guaiacol (VG)*.** 4-vinyl guaiacol places the vinyl group *para* to the phenolic OH which generates two stable conformers (Z*-VG** and ***E*-VG**), both of which possess a $OH\cdots OCH_3$ intramolecular H-bond. The two conformers were identified in the rotational spectra using the conformer-specific technique Strong-field coherence breaking (SFCB)[11,12] (see Figures 1c and 1d). Further details of these measurements are provided in Supplementary information. Finally, an estimation of the experimental population distribution 75(3):25(4) (***Z*-VG**:***E*-VG**) was determined by fitting experimental integrated line intensities to extract relative densities.

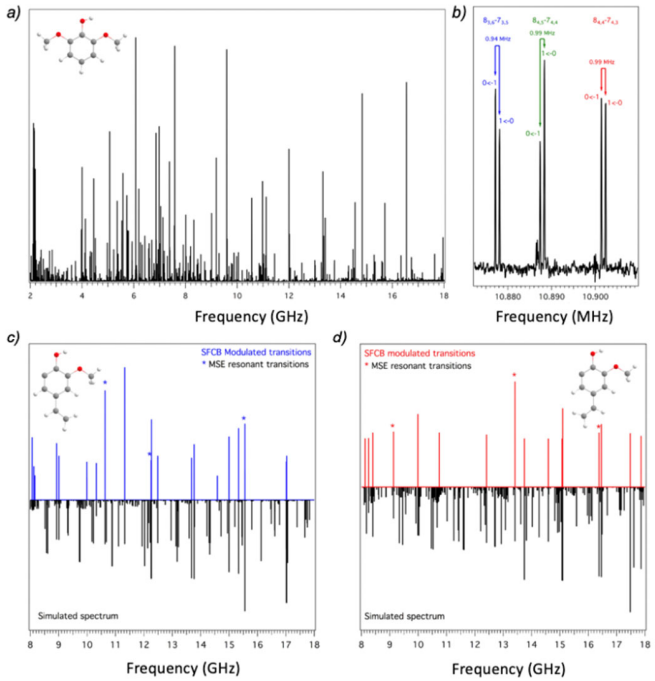

Figure 1. *(a)* Experimental CP-FTMW rotational spectrum of syringol (**S**), one of the model components of lignin studied here. *(b)* An expanded view highlights the tunneling doublets present in the $8_{3,6}$-$7_{3,5}$, $8_{4,5}$-$7_{4,4}$, and $8_{4,4}$-$7_{4,3}$ rotational transitions due to the internal rotation of the hydroxyl group. *(c and d)* Transitions (in red and blue) whose intensities are modulated by the Strong-Field Coherence Breaking (SFCB) technique. The best-fit calculated spectra are shown below in black. The resonant transitions chosen for coherence breaking are identified with an asterisk (*) in the spectra. The figure shows the power of the technique to selectively distinguish transitions due to each of the individual conformers of *(c)* ***Z*-VG** (blue) and *(d)* ***E*-VG** (red).

Internal Dynamics

The internal dynamics of lignin is potentially very rich due to the presence of hydroxy (-OH), methoxy ($-OCH_3$), vinyl ($-CH{=}CH_2$) and in some cases additionally methyl ($-CH_3$) groups. For **G,** which represents the simplest scaffold of lignin, no internal dynamics were observed because the juxtaposition of the OH and OCH_3 groups locks in their relative orientation. Moreover, the V_3 barrier for the methyl group in OCH_3 is estimated to be ~1000 cm^{-1}, thus we are not able to experimentally resolve the splittings. However, in **S**, the addition of another methoxy group in position 6 produces a symmetric double minimum for OH internal rotation, leading to tunneling splittings in the μ_a-type rotational transitions. Similar behavior was observed in phenol,[15,16] 2,6-difluorophenol,[17] propofol[18] and its symmetric *para*-derivatives.[19–21] Note that '*a*' and '*b*' axes are switched in **S** relative to phenol, its parent molecule.

A quantitative description of the OH tunneling process was carried out using Meyer's one-dimensional flexible model[22]. The barrier height to OH internal rotation was adjusted to reproduce the observed tunneling splitting and inertial defect, taking into account the most significant structural relaxations. The best-fit values obtained are V_2 = 1975 cm^{-1} and ΔE_{01} = 0.47569(78) MHz. Noticeably, V_2 is remarkably close to the theoretical value of 1962 cm^{-1} obtained at the DFT-B3LYP /def2tzvp method level of theory. Details of the methodology used can be found in the SI. We leave a discussion comparing tunneling barriers in related molecules to the following *OH barrier section*.
On the other hand, the methyl group present in **MG** on the phenyl ring *para* to the OH substituent produces an observable splitting due to internal rotation. The V_3 barrier for this methyl group was estimated from the fit to be 67.3 cm^{-1}, by combining values with structural parameters to evaluate the 1st-order dimensionless perturbation coefficients for the threefold barrier introduced by Herschbach[23] (for more details see SI) This value is in good correspondence with the 81 cm^{-1} calculated barrier height, and with the experimental value previously obtained by Dean *et al*.[8] using laser-induced fluorescence (V_3 = 70 cm^{-1}). Analogous values of V_3 barriers were observed in related systems, as *cis*-*m*-methyl anisole (55.7 cm^{-1})[24] and *p*-cresol (V_3 = 18 cm^{-1}; V_6 = -13.8 cm^{-1}).[25] Finally, the *p*-vinyl group of **VG** breaks the symmetry producing two different confomers (***Z*-VG** and ***E*-VG**). Hence, no tunneling splittings were observed in its rotational spectrum.

OH barrier (S). From a dynamic point of view, the ability of **S** to undergo tunneling between the two in-plane OH torsional positions is intriguing. In the microwave spectrum, resolved tunneling splittings were observed in the ^aR-type transitions due to the OH group tunneling through its torsional barrier between equivalent in-plane geometries. The selection rules indicate that these involve lower-to-upper and upper-to-lower tunneling transitions, producing a splitting (~1.0 MHz) that is twice the energy separation between the 0$^+$ and 0$^-$ tunneling levels (ΔE$_{01}$ = 0.47569(68) MHz).
The OH torsional barrier height can be compared to previous studies on phenolic derivatives. The experimental barrier height of **S** (1975 cm^{-1}) is greater than the barriers determined for phenol (1213(18) cm^{-1}),[15,16,26] propofol (Gg) (905-940 cm^{-1}),[18] and *p*-hydroxypyridine (1513(10) cm^{-1}).[21] The magnitude of the internal rotor barrier is affected by the electron donor/acceptor capabilities of the exocyclic substituent; for example, in *p*-hydroxypyridine the electron-withdrawing effect of the nitrogen atom is responsible for increasing the barrier relative to phenol, whereas in propofol the electron-donation from the two isopropyl groups causes the barrier height to be reduced considerably. In **S**, the main reason for the significant increase in the barrier height is the additional stabilization present at planar geometries from the intramolecular H-bond between the OH group and its neighboring methoxy groups. The comparison with phenol thus suggests that the stabilization of the in-plane geometry for the OH group is about two-thirds due to electronic effects of hyperconjugation of the OH group with the ring (~1200 cm^{-1}), and one-third due to the stabilization of the H-bond itself (~775 cm^{-1}).
The effect of this increased barrier on the OH tunneling splitting is dramatic, since in phenol, the tunneling splitting is ~111 MHz, while in **S**, it drops to ~1 MHz. Given this small splitting, it is not surprising that zero-point shifts induced by the presence of even a single ^{13}C in an asymmetric position is sufficient to quench tunneling.

Structural Analysis

The four model lignin molecules studied in this work are very similar structurally. All the structures have in common the intramolecular OH···OCH$_3$ H-bond which occurs within the plane of the ring and locks the molecule into a planar heavy-atom geometry. The literature provides many examples of this pattern[27] with exceptions appearing only when another functional group(s) competes for hydrogen bonding.[28]
Using ^{13}C isotopologue data, we were able to determine experimental structures for the phenyl ring of **G**, the starting framework for the molecules studied. Table 2 shows the substitution geometry (r_S)[29] with analogous values to the ones obtained by Gurusinghe *et al*.,[9] and a least-squares fitted ground state experimental structure (r_0). Unfortunately, the two geometries exhibit significant discrepancies between them. For example, the shortest bond length $r_{C(1)-C(2)}$ extracted from a Kraitchman analysis is the longest bond in the effective structure (Table 2). It is therefore difficult to draw conclusions *a priori*.

Table 2. Experimental and calculated structural parameters for **G** (distances in Å and angles in degrees).

	r_S[a]	r_0	MP2[b]	B3LYP[b]	B3LYP-D3BJ[c]	MP2[d]
$r_{C(1)-C(2)}$	1.355(16)	1.415(20)	1.411	1.404	1.403	1.404
$r_{C(2)-C(3)}$	1.412(19)	1.393(28)	1.397	1.386	1.388	1.391
$r_{C(3)-C(4)}$	1.419(5)	1.410(31)	1.404	1.395	1.396	1.398
$r_{C(4)-C(5)}$	1.394(3)	1.390(49)	1.397	1.385	1.387	1.391
$r_{C(5)-C(6)}$	1.394(4)	1.400(39)	1.401	1.394	1.394	1.396
$r_{C(6)-C(1)}$	1.396(4)	1.388(31)	1.393	1.383	1.384	1.387

[a] Substitution structure obtained by Gurusinghe *et al*.[9]
[b] MP2/6-311G(d,p) basis set.
[c] B3LYP-D3BJ/def2tzvp level.

[d] MP2/aug-cc-pvtz level.

The inconsistencies arising from a substitution geometry method such as Kraitchman analysis are a consequence of the large errors that occur in the positions of atoms that are close to an inertial axis (C(2) and C(3) in this case). Hence, we have chosen the experimental effective geometry (r_0) as a reference for drawing conclusions concerning the structural parameters. To investigate and draw structural conclusions, the two geometries were compared with the structure computed at the DFT B3LYP-D3BJ/def2tzvp level, which reproduces the rotational constants quite well. The effective structure and the computationally simulated geometry are in close agreement with one another. To confirm this fact, a range of computational methods were used and all of them have the same behavior (Table 2).

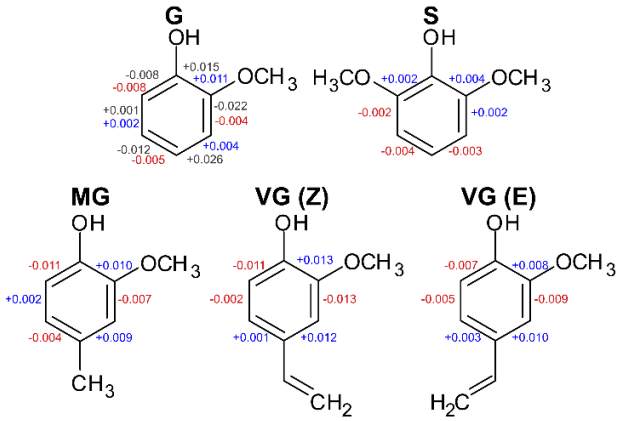

Figure 2. Summary of bond changes relative to the average bond length $r_{C\text{-}C}$. The values have been obtained from the experimental effective structure (**G**) and are indicated in black. The computed molecular geometries of **G**, **S**, **MG** and **VG** at B3LYP-GD3BJ/def2tzvp are also shown. Color coding identifies an increase in blue and a decrease in red.

As shown in Figure 2 and Table 2, substitution of OH and OCH_3 groups on the phenyl ring of **G** distorts the ring itself away from six-fold symmetry. While some $r_{C\text{-}C}$ bond lengths are lengthened, others are shortened. Although the uncertainty in the experimentally determined bond lengths (20-50 mÅ) is comparable to the magnitude of lengthening/shortening (20 mÅ), the pattern of lengthening and shortening shows that **G** exhibits a *bond length alternation*. This chemical phenomenon takes place in (multi)-substituted benzenes and in benzene rings fused to small saturated rings. Despite its interest, there are not many cases where it has been possible to observe this effect experimentally.[30–33]

As a result, it is interesting to assess in detail the structural changes induced by the addition of functional groups, a methoxy group (**S**), methyl group (**MG**) or vinyl group (**VG**), on the structures and bonding. For this purpose and due to the absence of experimental data on isotopologues, we used calculations at the B3LYP-GD3BJ/def2tzvp level which are the ones that best reproduce the experimental constants. **MG** and **VG** (to a lesser degree) also exhibit *bond length alternation*. In order to get a more comprehensive view of this effect, we optimized the structures of other structurally similar molecules at the same level of theory, including phenol,[26] anisole,[34] anethole (*E-anti*) and *p*-vinylphenol (*anti*).[35] None of these molecules exhibit the *bond length alternation* to any significant extent (Figure S2). We surmise on this basis that the asymmetry of the single methoxy substituent propagates through the structure and is dominant over the effects of the OH or vinyl groups.

In the three structures **G**, **MG** and **VG**, the longest bond $r_{C\text{-}C}$ in the phenyl ring is that between the two substituted carbons ($r_{C(1)\text{-}C(2)}$). The adjacent bonds are the shortest, showing either the effects of the steric crowding between these two groups or the hyperconjugation of the oxygen lone pair with the aromatic ring. The H-bond between the hydroxy and the methoxy groups does not seem able to compensate for the effect of the methoxy group on the ring. When combined with the shortened $r_{C(4)\text{-}C(5)}$ bond on the opposite side of the ring, this bond alternation indicates that this resonance structure, with double bond positions shown in Figure 2, gains in weight over its alternative, in which the single and double bonds are swapped in the ring.

In **S**, the presence of the second methoxy group brings a near two-fold symmetry to the structure. Indeed, when tunneling of the OH group is considered, the molecule is effectively C_{2v} symmetry. Even in the optimized structure at one of the tunneling minima (as shown in Figure 2), the bond lengths $r_{C\text{-}C}$ in the aromatic ring are still nearly equivalent. It is clear that the principal motion associated with tunneling is undoubtedly internal rotation of the OH group in **S**. However, the heavy atoms in the oxygenated substituents also undergo small shifts in position. Based on the optimized geometry for **S** in one of its tunneling minima (shown in Figure 2), the most significant changes are in the $r_{C(2/6)\text{-}O}$ bond lengths and $\angle_{C(1)C(2)O(2)}$ bond angles of the two methoxy groups, which expand by 10 mÅ and 2 degrees, respectively, when the OCH_3 acts as H-bond acceptor.

Conclusion

We have carried out broadband microwave spectroscopy on guaiacol (**G**), 4-methyl guaiacol (**MG**), syringol (**S**), and 4-vinylguaiacol (**VG**) under jet-cooled conditions in the gas phase. An effective geometry (r_0) was determined for **G**, allowing the experimental observation of the bond length alternation in the phenyl ring. **MG** and **VG** present a similar distortion of the phenyl ring; thus, one can conclude that the polar substituents, particular methoxy, dictate the structural shifts from the unsubstituted aromatic ring. Surprisingly, the vinyl group, which is asymmetrically conjugated with the phenyl ring, does not distort the ring in any significant way. The most significant change between the ***Z*-VG** and ***E*-VG** conformers is a slight modulation in the length of the $r_{C(1)\text{-}C(2)}$ and $r_{C(5)\text{-}C(6)}$ bonds.
In the case of **S**, tunneling splittings due to OH hindered rotation were observed. A simple 1D model for the process leads to a value of V_2 = 1975 cm^{-1} for this barrier. This value is 50% greater than phenol's barrier, due to the presence of the methoxy groups, which engage in intramolecular H-bonding with the OH group.
The present work demonstrates the value of a combination of rotational spectroscopy with high level calculations as an important tool to structurally characterize the components of lignin. It opens the possibility of testing larger lignin oligomers, which may produce these molecules as pyrolysis intermediates. The pyrolysis of **S** represents a natural extension of earlier work at Purdue on the pyrolysis of 2-methoxy furan[36] and **G**.[37] The presence of two methoxy groups in **S** opens the way for a richer set of pyrolysis pathways via loss of one or two methyl groups.

Experimental Section

Experimental Details

The broadband rotational spectra of **G** (98%), **S** (99%), **MG** (98%), and **VG** (98%) were recorded in the 2-18 GHz frequency range using a CP-FTMW spectrometer. The instrument has been described in detail elsewhere.[38] All samples were purchased from Sigma Aldrich and introduced into the gas phase by placing a small amount in a stainless-steel sample holder immediately before a solenoid-driven pulsed valve (Parker series 9). The sample holder was heated to transfer the substance into the gas phase. The solenoid valve was triggered at 10 Hz repetition rate using a home-made driver. The experimental timing scheme allowed the collection of 20-30 molecular free induction decays (FIDs) per gas pulse. The molecular emission was phase coherently averaged in the time domain and digitized for 16 μs with a 13 GHz, 40 GS/s real time digitizer (Guzik ADC6131). A corrected FID that removes baseline shifts between the interleaved analog-to-digital converters was obtained using a custom Matlab routine. The data was filtered with a Kaiser-Bessel filter and a Fast Fourier transform (FFT) was performed to obtain the frequency domain spectrum.

Computational Details. All electronic structure calculations were performed using the Gaussian16 program suite.[39] Geometry optimizations for all the molecules were carried out using a range of methods in order to assess the spectroscopic parameters and structural arrangements. Density functional theory (DFT) calculations that employed the B3LYP functional, including Grimme's dispersion[40] correction and Becke-Johnson damping,[41] were carried out using the Karlsruhe basis set, def2-TZVP. This level of theory has been shown to yield rotational constants that are in close agreement with experiment.[42,43] These results were compared with MP2/aug-cc-pVTZ calculations..

Acknowledgements

AOHC, SMF, and TZ gratefully acknowledge support for this research from the Department of Energy Basic Energy Sciences, Chemical Sciences Division under Grant No. DE-FG02-96ER14656. TSZ acknowledges support from the U.S. DOE, Office of Science, Office of Basic Energy Sciences during manuscript preparation at Sandia. Sandia National Laboratories is a multi-mission laboratory managed and operated by National Technology and Engineering Solutions of Sandia, LLC., a wholly owned subsidiary of Honeywell International, Inc., for the U.S. DOE National Nuclear Security Administration under contract DE-NA0003525. IU is grateful for support of FPU grant during her visit to Purdue University. EJC thanks for the support received from the MINECO (CTQ2017-89150-R and PID2020-117892RB-I00), Basque Government (IT1162-19 and PIBA 2018-11), the UPV/EHU (PPG17/10, GIU18/207), CSIC (PIC2018, LINKA20249). Computational resources and laser facilities of the UPV/EHU (SGIker) and CESGA were used in this work. We thank Prof. Assimo Maris (University of Bologna) for sharing her valuable experience on internal dynamic motions.

[1] A. Barakat, F. Monlau, J. P. Steyer, H. Carrere, *Bioresour. Technol.* **2012**, *104*, 90–99.

[2] G. Jiang, D. J. Nowakowski, A. V Bridgwater, *Thermochim. Acta* **2010**, *498*, 61–66.

[3] A. U. Buranov, G. Mazza, *Ind. Crops Prod.* **2008**, *28*, 237–259.

[4] J. Huang, X. Li, D. Wu, H. Tong, W. Li, *J. Renew. Sustain. Energy* **2013**, *5*, 43112.

[5] V. K. Ponnusamy, D. D. Nguyen, J. Dharmaraja, S. Shobana, J. R. Banu, R. G. Saratale, S. W. Chang, G. Kumar, *Bioresour. Technol.* **2019**, *271*, 462–472.

[6] M. P. Vinardell, M. Mitjans, *Int. J. Mol. Sci.* **2017**, *18*, DOI 10.3390/ijms18061219.

[7] M. Azadfar, A. H. Gao, S. Chen, *Int. J. Biol. Macromol.* **2015**, *75*, 58–66.

[8] J. C. Dean, P. Navotnaya, A. P. Parobek, R. M. Clayton, T. S. Zwier, *J. Chem. Phys.* **2013**, *139*, 144313.

[9] R. M. Gurusinghe, A. Fox-Loe, M. J. Tubergen, *J. Mol. Struct.* **2021**, *1246*, 131233.

[10] J. A. Ruiz-Santoyo, M. Rodríguez-Matus, J. L. Cabellos, J. T. Yi, D. W. Pratt, M. Schmitt, G. Merino, L. Álvarez-Valtierra, *J. Chem. Phys.* **2015**, *143*, 094301-1–9.

[11] A. O. Hernandez-Castillo, C. Abeysekera, B. M. Hays, T. S. Zwier, *J. Chem. Phys.* **2016**, *145*, DOI 10.1063/1.4962505.

[12] S. M. Fritz, A. O. Hernandez-Castillo, C. Abeysekera, B. M. Hays, T. S. Zwier, *J. Mol. Spectrosc.* **2018**, *349*, 10–16.

[13] H. M. Pickett, *J. Mol. Spectrosc.* **1991**, *148*, 371–377.

[14] R. K. Thomas, *Phys. Bull.* **1975**, *26*, 501–501.

[15] E. Mathier, D. Welti, A. Bauder, H. H. Günthard, *J. Mol. Spectrosc.* **1971**, *37*, 63–76.

[16] N. W. Larsen, E. Mathier, A. Bauder, H. H. Günthard, *J. Mol. Spectrosc.* **1973**, *47*, 183–188.

[17] M. K. Jahn, D. A. Dewald, D. Wachsmuth, J. U. Grabow, S. C. Mehrotra, *J. Mol. Spectrosc.* **2012**, *280*, 54–60.

[18] A. Lesarri, S. T. Shipman, J. L. Neill, G. G. Brown, R. D. Suenram, L. Kang, W. Caminati, B. H. Pate, *J. Am. Chem. Soc.* **2010**, *132*, 13417–13424.

[19] T. Motoda, M. Onda, I. Yamaguchi, *Chem. Lett.* **1986**, *15*, 57–60.

[20] N. W. Larsen, *J. Mol. Struct.* **1986**, *144*, 83–99.

[21] R. Sanchez, B. M. Giuliano, S. Melandri, W. Caminati, *Chem. Phys. Lett.* **2006**, *425*, 6–9.

[22] R. Meyer, *J. Mol. Spectrosc.* **1979**, *76*, 266–300.

[23] D. R. Herschbach, *J. Chem. Phys.* **1959**, *31*, 91–108.

[24] L. Ferres, W. Stahl, H. V. L. Nguyen, *J. Chem. Phys.* **2018**, *148*, DOI 10.1063/1.5016273.

[25] G. Myszkiewicz, W. L. Meerts, C. Ratzer, M. Schmitt, *J. Chem. Phys.* **2005**, *123*, DOI 10.1063/1.1961615.

[26] N. W. Larsen, *J. Mol. Struct.* **1979**, *51*, 175–190.

[27] E. J. Cocinero, A. Lesarri, P. Écija, J.-U. Grabow, J. A. Fernández, F. Castaño, *Phys. Chem. Chem. Phys.* **2010**, *12*, 12486–12493.

[28] E. J. Cocinero, A. Lesarri, P. Écija, F. Basterretxea, J. A. Fernández, F. Castaño, *J. Mol. Spectrosc.* **2011**, *267*, 112–117.

[29] C. C. Costain, *J. Chem. Phys.* **1958**, *29*, 864–874.

[30] I. Uriarte, F. Reviriego, C. Calabrese, J. Elguero, Z. Kisiel, I. Alkorta, E. J. Cocinero, *Chem. - A Eur. J.* **2019**, *25*, 10172–10178.

[31] A. Maris, B. M. Giuliano, S. Melandri, P. Ottaviani, W. Caminati, L. B. Favero, B. Velino, *Phys. Chem. Chem. Phys.* **2005**, *7*, 3317–3322.

[32] W. Caminati, in *Handb. High-Resolution Spectrosc.*, **2011**.

[33] S. Saxena, S. Panchagnula, M. E. Sanz, C. Pérez, L. Evangelisti, B. H. Pate, *ChemPhysChem* **2020**, *21*, 2579–2584.

[34] O. Desyatnyk, L. Pszczółkowski, S. Thorwirth, T. M. Krygowski, Z. Kisiel, *Phys. Chem. Chem. Phys.* **2005**, 1708–1715.

[35] P. J. Morgan, D. M. Mitchell, D. W. Pratt, *Chem. Phys.* **2008**, *347*, 340–345.

[36] C. Abeysekera, A. O. Hernandez-Castillo, J. F. Stanton, T. S. Zwier, *J. Phys. Chem. A* **2018**, *122*, 6879–6885.

[37] A. M. Scheer, C. Mukarakate, D. J. Robichaud, M. R. Nimlos, G. B. Ellison, *J. Phys. Chem. A* **2011**, *115*, 13381–13389.

[38] S. M. Fritz, B. M. Hays, A. O. Hernandez-Castillo, C. Abeysekera, T. S. Zwier, *Rev. Sci. Instrum.* **2018**, *89*, 093101.

[39] M. J. Frisch, G. W. Trucks, H. B. Schlegel, G. E. Scuseria, M. A. Robb, J. R. Cheeseman, G. Scalmani, V. Barone, G. A. Petersson, H. Nakatsuji, others, *Gaussian Inc. Wallingford CT* **2016**, *1*.

[40] S. Grimme, *Wiley Interdiscip. Rev. Comput. Mol. Sci.* **2011**, *1*, 211–228.

[41] S. Grimme, S. Ehrlich, L. Goerigk, *J. Comput. Chem.* **2011**, *32*, 1456–1465.

[42] D. Zhang, S. Bocklitz, T. S. Zwier, *J. Phys. Chem. A* **2016**, *120*, 55–67.

[43] A. O. Hernandez-Castillo, C. Abeysekera, B. M. Hays, I. Kleiner, H. V. L. Nguyen, T. S. Zwier, *J. Mol. Spectrosc.* **2017**, *337*, 51–58.